LAWRENCE
LIVERMORE
NATIONAL
LABORATORY

LLNL-JRNL-491161

First-principles molecular dynamics simulations of condensed phase V-type nerve agent reaction pathways and energy barriers

R. H. Gee, I. W. Kuo, S. C. Chinn, E. Raber

July 20, 2011

Physical Chemistry Chemical Pysics

Disclaimer

First-principles molecular dynamics simulations of condensed phase V-type nerve agent reaction pathways and energy barriers

Richard H. Gee,[†] I-Feng W. Kuo,[†] Sarah C. Chinn,[†] Ellen Raber[‡]

†Chemical Sciences Division, Lawrence Livermore National Laboratory, Livermore, California 94550, USA

[‡]Global Security Directorate, Lawrence Livermore National Laboratory, Livermore, California 94550, USA

e-mail of corresponding authors:

gee10@llnl.gov

Abstract

Computational studies of condensed phase chemical reactions are challenging due in part to complexities in understanding the effects of the solvent environment on the reacting chemical species. Such studies are further complicated due to the demanding computational resources required to implement high-level *ab initio* quantum chemical methods when considering the solvent explicitly. Here we use first-principles molecular dynamics simulations to examine condensed phase decontamination reactions of V-type nerve agents in an explicit aqueous solvent. Our results include a detailed study of hydrolysis, base-hydrolysis, and nucleophilic oxidation of both VX and R-VX, as well as their protonated counterparts (i.e., VXH^+ and R-VXH^+). The decontamination mechanisms and chemical reaction energy barriers, as determined from our simulations, are found to be in good agreement with experimental results. The results demonstrate the applicability of using such simulations to assist in the understanding of new decontamination technologies or other applications that require computational screening of condensed phase chemical reaction mechanisms.

I. Introduction

Solvent effects are of primary importance in chemical reactivity and pose significant challenges when approached computationally. Additionally, realistic depictions of bond making and breaking events in the condensed phase, which result in significant changes to the electronic structure of the reacting species can be problematic. Further, it is well known that the reactions rates in gas phase and in solution can differ significantly,[1-3] thus illustrating the importance of solvent in determining the governing reaction mechanisms and corresponding reaction rate. However, most computational studies of condensed phase chemical reactions implement continuum solvation models, which treat the solvent implicitly, and are therefore unsuitable when knowledge of the explicit behavior of the surrounding solvent is deemed to be important. Therefore, an explicit treatment of the solvent surroundings becomes necessary. However, an explicit treatment of the condensed phase leads to an enormous number of degrees of freedom, which often make a first-principles computational study of condensed phase chemical reaction intractable. On the other hand, advances in high performance computing coupled with sophisticated rare-event sampling techniques[4,5] can aide in making such approaches feasible. The viability of such an approach however, is dependent on the ability to represent each state of the reacting system statistically, which in turn is dependent on the availability of computational resource and computational efficiency of the algorithms employed.

To this end, we have endeavored to explore condensed phase decontamination reactions of V-type nerve agents in an explicit aqueous solvent using first-principles molecular dynamics simulations. Specifically, we have examined decontamination reactions of O-ethyl S-[2-(diisopropylamino)ethyl] methylphosphonothioate (VX) and its isomeric analog O-isobutyl S-[2-(diethylamino)ethyl] methylphosphonothioate (R-VX) both in their neutral and

protonated states. The precedence for such a study is borne out of the fact that in recent years there have been increased concerns regarding terrorist activities and the utilization of chemical warfare agents.[6] Restoration and remediation efforts rely on a complete understanding of the reaction chemistry of the agents with potential decontaminants. In cases when traditional decontamination approaches are not feasible or desirable due to unfavorable reaction effects (e.g. corrosion of the material to be contaminated), alternative approaches must be evaluated. While such information can be obtained experimentally through trial and error experiments, they are limited to facilities capable of handling such agents with the appropriate safety precautions. Due to the hazardous nature of the work, it is desirable to reduce the number of experiments necessary to fully understand how agents interact with decontaminating solutions by first simulating the reaction chemistry. Many theoretical studies of VX decontamination have been performed,[7-9] but none in which the solvent has been treated explicitly, therefore eliminating the possibility of identifying important solvent mediation effects. Furthermore, such systems have been extensively studied experimentally,[10-20] thus providing a significant body of work to validate our model approach. For example, Yang *et al.*[17] has studied the competitive bond cleavage mechanism between P-S and P-O for VX, and determined the activation energies at pH 11 to be 12.6 and 11.1 kcal/mol, respectively. Similar activation energies have also been reported for VX decomposition on concrete.[21,22] In general, V-type nerve agents have been shown to be effectively decontaminated via nucleophilic substitution reactions.[10,14,16]

In this work, we present our first-principles simulation results for a variety of decontamination mechanisms and chemical reaction energy barriers of V-type nerve agents in the presence of explicitly represented water. These results include reaction mechanisms and reaction energy barriers for reactions centered not only at the phosphorous atomic center, but

the sulfur, nitrogen and carbon atomic centers as well. Further, simulation results are also presented for our computational investigation of the recently hypothesized mechanism of VX hydrolysis via an autocatalytic hydrolysis pathway,[15,19,23] thus, emphasizing the importance of including the solvent explicitly in condensed phase theoretical studies of chemical reactions.

II. Methods

a. First-principles molecular dynamics (FPMD) simulations.

All simulations were carried out using the program CP2K.[24] The forces were computed via the QuickStep[25] module, which contains an accurate and efficient implementation of density functional theory using dual basis sets of Gaussian type orbitals (TZV2P) and plane waves (expanded to E_{cut} = 280 Ry) for the electron density. Only the valence electrons were considered explicitly while the core electronic states were represented via a Goedecker–Teter–Hutter pseudopotentials.[26] Exchange and correlation energy was computed within the GGA approximation using the PBE functional.[27] With a chosen molecular dynamics time step of 0.5 fs, the wavefunction was minimized to a tolerance of 10^{-6} Hartree. All simulations were performed in the canonical ensemble at 350 K by coupling Nosé–Hoover chain thermostats with characteristic frequencies of 2000 cm^{-1} to every degree of freedom.[28]

b. Metadynamics.

The metadynamics rare event sampling technique[5] has been employed here to sample the reactive Gibbs free energy surface where VX and R-VX (both neutral and protonated species) can interact with hypochlorite anion (aqueous bleach) in an aqueous environment. Metadynamics is a nonequilibrium method that allows for the system to escape minima in order to sample the rest of the free energy surface on a time scale that is accessible by present day computers.[29,30] Metadynamics has been used in a number of applications, including the

investigation of bacterial chloride channels,[31] deprotonation of formic acid,[32] and flexible ligand docking.[33] The method is based on the assumption that it is possible to define a set of collective coordinates that can distinguish between reactants and products and can sample the low-energy reaction paths. Collective variables (CVs) must be functions of the ionic coordinates; examples include bond lengths and coordination numbers, etc. As a molecular dynamics simulation is performed, history-dependent repulsive potential is built up in low-energy wells by adding a biasing potential term along the CVs at each metadynamic step in the form of a small Gaussian "hill" (Eq. 1). As the hills build up along the CVs, the system is forced to escape local minima and to explore higher energy regions of the Gibbs free energy surface (FES). In the limit of infinite time, the biasing potential exactly cancels the underlying FES along the CVs (Eq. 2):

$$V_{bias}(\mathbf{s},t) = \sum H \exp\left(\frac{\left|\mathbf{s} - s(t_i)\right|^2}{2\omega^2} \right) \tag{1}$$

$$F(\mathbf{s}) = -V_{bias}(\mathbf{s},t)_{t\to\infty} \tag{2}$$

V_{bias} is the repulsive biasing potential term, which is a function of the CVs, **s**, and time, *t*, with hill parameters having height *H* and width ω. The FES, *F*(**s**), can be reconstructed along the CVs given a sufficient amount of time.

c. Nudged-Elastic-Band.

To compliment the results obtain from metadynamics simulations, when necessary, an improved version of the Nudged-Elastic-Band (NEB) method, the *improved-tangent* NEB (IT-NEB),[4] was also employed to locate the minimum energy pathways (MEP) for the condensed phase chemical reactions studied here. With this approach, the MEP is found by constructing a set of replicas (images) of the system between the initial and final states (here we use 32 replicas throughout). A spring interaction (where the force constant, *k* was chosen as $1\text{x}10^{-4}$

Hartree/Bohr^2) between adjacent images is added to ensure continuity of the path, thus mimicking an elastic band. An optimization of the band, involving the minimization of the force acting on the images, brings the band to the MEP. For the IT-NEB method, as implemented in this study, each replica was relaxed until the maximum force and *rms* force acting on an atom is ≤ 0.001 and ≤ 0.0005 Ha/Å, respectively. The MEP is then used as an estimate for the energy barrier for transitions between the initial and final states.

III. V-type nerve agent model systems and computational details

All systems (ensembles) studied here consisted of a single V-type nerve agent molecule and 76 water molecules in a 14 Å X 14 Å X 14 Å box with periodic boundary conditions applied in three dimensions (herein referred to as the "core-ensemble"). The V-type nerve agents studied here include either MeP(O)(OR)($SCH_2NR'_2$), VX (R = C_2H_5; R' = *i*-C_3H_7) or its isomeric analog R-VX ("Russian VX," R = *i*-C_4H_9; R' = C_2H_5), see Figure 1. Protonated VX and R-VX counterparts were also studied. The protonated species (VXH^+ or R-VXH^+) were studied due to the propensity for either of these species to protonate (at the nitrogen atom) in neutral or basic solutions (pK_a of VX = 8.6 @ 25 ^oC).[34] Each of the condensed phase system studied here were initially constructed using the Materials Studio[35] software package and equilibrated with classical molecular dynamics utilizing the COMPASS force field[36] before any FPMD simulations were performed. Following the "classical" equilibration, each system studied was equilibrated in FPMD simulations with CP2K for 5 ps before any metadynamics simulations were performed to study the condensed phase chemical reactions.

a. Oxidation of V-type nerve agents with hypochlorite anion.

For our study of condensed phase oxidation reactions of V-type nerve agents, a single hypochlorite anion (ClO^-) and a single sodium cationic counter ion, (Na^+) were added to the core-ensemble (where the density of the simulation box is $\rho = 1.03539$ for V-type nerve agents and $\rho = 1.036$ for protonated V-type nerve agents). The CV for the metadynamics simulations used to study the oxidation reactions of VX (or VXH^+) and R-VX (or R-VXH^+) with the hypochlorite ion (ClO^-) was chosen as the distance between the oxygen atom of the hypochlorite anion and the atom center of interest in the V-type nerve agent molecule (e.g., phosphorus, sulfur, carbon, etc.). In addition, several different metadynamics parameters (hill height and width) were tested, were the final parameters were chosen as; $H = 1.0 \times 10^{-3}$ hartree, $\omega = 0.1$ Bohr, and where hills, H, were added every 15 MD steps (time step = 0.5 fs).

Many of the reactions studied using metadynamics simulations were also studied using the IT-NEB approach in order to improve our confidence in obtaining appropriate reaction energy barriers in the transition state region.[37] The replicas (the atomic coordinates) used in the IT-NEB simulations were taken directly from the metadynamics trajectories along the identified reaction coordinate of the reaction. Specifically, 16 replicas where extracted from the initial state ("reaction" side of the reaction coordinate) and 16 replicas from the final state ("product" side of the reaction coordinate), thus providing a total number of 32 replicas, which define the reaction coordinate studied.

b. Hydrolysis of VX in basic solutions.

FPMD condensed phase metadynamics simulations of base hydrolysis were performed by adding a single hydroxide anion (OH^-) to the core-ensemble of VX described in section III. Here the CV was chosen as the bond distance between sulfur carbon (S-C) atoms the VX

molecule. The metadynamics parameters (hill height, *H*; width, ω, etc.) were chosen as; *H* = 5.0 X 10^{-4} Hartree, ω = 0.1 Bohr, and where hills, *H*, were added every 30 MD steps (15 fs).

c. Autocatalytic hydrolysis of VX.

It has been proposed that VX or R-VX may "autocatalytically" hydrolyze.[15] To study the plausibility of such a mechanism, we performed FPMD simulations where the free energy surface is sampled via metadynamics on a gas phase cluster containing a single water and VX molecule, similar to that shown in Figure 8a, as well as a fully condensed phase simulation using the core-ensemble described in section III above. Two CVs were chosen to study the autocatalytic hydrolysis of VX; the CVs are defined as the distance between the phosphorus (CV_1) or the nitrogen (CV_2) atomic centers, and selected oxygen of a water molecule in close proximity to the VX molecule (see Figure 8a). The parameters for the biasing potential (hill height, *H*; width, ω, etc.) were the same as those defined in section IIIa.

IV. Results

a. VX and R-VX hypochlorite decontamination reactions.

The main focus of this paper is to demonstrate the feasibility of employing FPMD simulation approaches to study condensed phase decontamination reactions of V-type nerve agents via hypochlorite (ClO^-) oxidation. Specifically, condensed phase FPMD metadynamics and IT-NEB simulations of VX (or VXH^+) and R-VX (or R-VXH^+) with the hypochlorite ion (ClO^-) were performed to ultimately identify decontamination degradation pathways and oxidation reaction energy barriers. Further, when possible, the results of our simulations are compared to experiment to validate the computational approach.

We first start by looking at hypochlorite reaction with VX or R-VX at both the nitrogen (N-centered) or sulfur (S-centered) atomic centers. Figure 2 shows the free energy as a function of distance between the hypochlorite oxygen and nitrogen or sulfur distance as determined by metadynamics simulations (see section IIIa). The resultant N-centered reaction potential energy barrier (PEB) for the hypochlorite reaction for both VX and R-VX were found to be similar, 11.5 and 10 kcal/mol, respectively. However, the S-centered hypochlorite reaction PEB for VX and R-VX was found to differ by >10-15 kcal/mol, favoring the R-VX/hypochlorite reaction; compare the dashed and solid gray curves of Figure 2. Upon securitization of the S-centered "transition-state structure," it was found that a single water molecule mediates the reaction of the R-VX molecule (see Figure 3); no such structure was identified for the S-centered VX reaction. Two hypothesis are put forward to understand this; 1) the development of a solvent mediated transition-state structure for VX is sterically hindered by the presence of the more bulky *isopropyl* nitrogen moieties of VX versus the less bulky *ethyl* moieties of R-VX, or 2) the simulations are nonergodic (i.e., the simulations were not run sufficiently long so as to allow for the development of a "single water molecule mediated transition state structure" in VX (again in part due to the presence of the more bulky *isopropyl* groups in VX).[37] To this end, additional S-centered VX/hypochlorite simulations were performed, where the additional sampling eventually resulted in water mediated transition-state structure (see right panel of Figure 4 for an illustration). The additional VX sampling required to identify the water mediated transition-state structure lend credence to the hypothesis that the more prominent steric effect found in VX ultimately impede the development of solvent mediation effects important in chemical reactions.

Starting from the water mediated transition-state structures yielded from the above S-centered metadynamic simulations; we employed the IT-NEB approach to determine the S-

centered hypochlorite reaction PEBs for VX and R-VX. Specifically, the replicas used in the IT-NEB calculations were taken directly from the previously described metadynamics simulations. The S-centered reaction PEBs obtained from the NEB simulations for VX and R-VX are shown in Figure 5, and are found to be $\Delta H \approx 15$ and $\Delta H \approx 11$ kcal/mol, respectively. As a final note, reactions involving either of the two carbon atoms along the backbone of the V-type nerve agent molecules were found to be energetically prohibitive, where the reaction PEBs were found to be greater than 40 kcal/mol (see Table 1 for further details).

We next consider nucleophilic substitution reactions involving hypochlorite at the phosphorus atomic center (P-centered). The PEBs for reaction of hypochlorite with VX and R-VX, as well as the protonated VXH^+ and R-VXH^+ counterparts were determined. Reactions of protonated VX and R-VX were deemed to be important for two reasons; 1) experiments have shown that the solubility of VX is increased under acidic conditions, where the increased solubility is hypothesized to be due to protonation of the nitrogen,[15,16,18,19] and 2) during equilibration, many of the simulations showed spontaneous protonation at the nitrogen center of VX and R-VX under "neutral" pH conditions. Further, our simulations also show spontaneous protonation of the hypochlorite ion (the pKa of hypochlorite is reported as being ~7.5,[38] consistent with this observation). P-centered nucleophilic substitution reactions were found to proceed via a S_N2 type mechanism, where the tetra-coordinated phosphorus forms a trigonal bipyramidal transition state (the formation of a trigonal bipyramidal transition state has been reported elsewhere[39-42]). Further, FPMD simulations were performed on all V-type reactants (VX, VXH^+, R-VX and R-VXH^+), where either the thiolate and ethoxy phosphorus moieties were found to be in either the axial or equatorial position of the trigonal bipyramidal transition state structure that developed. For P-centered substitution reactions involving a P-SR bond cleavage mechanisms, we find a lowering in the PEB when the thiolate (-SR) moiety

is in the equatorial position as compared to axial position of the trigonal bipyramidal transition state structure; 12 versus 15 kcal/mol (see VX(P-S) entry in Table 1). This result is perhaps somewhat surprising when considering that in general, it is assumed that the most electronegative group (here the ethoxy moiety) prefer the axial position in the trigonal bipyramidal transition state, and is believed to be the most facile in this position. However, the thiolate is less basic than the ethoxy moiety, and thus may be considered a good leaving group.[43] Ultimately, this leads to a competition between cleavages of the P-O or P-S bonds, as seen here, as well as in the published literature.[9,40-44]

Table 1 summarizes our computed reaction PEBs for several important reactions. Several salient results are noteworthy; 1) based on our computed PEBs, the nitrogen atomic center is likely to be oxidized first in VX, however, for R-VX, both the nitrogen and the sulfur atomic centers show roughly equal probability of oxidation by ClO^-, 2) sulfur oxidation leads to P-S bond rupture, 3) nucleophilic substitution at the phosphorous atomic center leads to P-O or P-S bond cleavage, where the preference for P-O or P-S bond cleavage was found to depend on the orientation of the 'incoming' nucleophile to the phosphorous atomic center, 4) reactions at the carbon atomic centers along the backbone are energetically unfavorable (all carbon/hypochlorite reactions were found to have potential energy barriers of greater than 40 kcal/mol), and 5) our results are in excellent agreement with experimental base hydrolysis results.[15,20] Further, the fact that our calculated results for hypochlorite oxidation of V-type nerve agents are strikingly similar to the experimental results found for base hydrolysis is perhaps surprising, however, as mentioned above, we find from our simulations that it is not uncommon for the hypochlorite species to spontaneously protonate right before it oxidizes the V-type nerve agent, thus the actual oxidizing agent may be "chemically" very similar to an OH^- nucleophile.

To further elaborate the above reactions centered at either the 'N' or 'S' atomic centers, first consider reactions at the nitrogen atomic center. As was stated above (see Table 1), oxidation at the nitrogen center is energetically favorable (PEB < 12 kcal/mol), but only under relatively basic conditions (pH > 8) due to the propensity for VX and R-VX to protonate at pH < 8, thus, oxidation at the protonated nitrogen in either VXH^+ or $R\text{-}VXH^+$ was found to be energetically prohibited (PEB > 30 kcal/mol). Further, we performed additional FPMD metadynamics simulations where a second hypochlorite anion was introduced into the ensemble which contained the newly formed VX/nitrogen oxidation product (N-(2-((ethoxy(methyl)phosphoryl)thio)ethyl)-N-isopropylpropan-2-amine oxide) (see the center structure of Figure 6a). The newly added hypochlorite anion was found to react ('second' oxidation step) at the sulfur atomic center, with a relatively low energetic penalty (PEB of ~10 kcal/mol). Additionally, the P-S bond was found to simultaneously elongate as the sulfur is oxidized (see Figure 6), ultimately allowing for further hydrolysis to occur at the phosphorus center. The decontamination reaction mechanism of VX seen here is consistent with previously reported experimental results of VX nucleophile oxidation.[14] The above VX/hypochlorite reaction mechanism is illustrated schematically in Figure 6a, along with the actual simulation trajectory (Figure 6b). As seen from the simulation trajectory (Figure 6b), the distance between the hypochlorite oxygen and the nitrogen in the VX molecule (black curve) shows the occurrence of the reaction at ~5 ps into the simulation. Note, that the P-S bond distance is unaffected by the formation of the N-oxide product (see red curve); t=5-7ps). At around 5 ps a second ClO^- was added to the ensemble containing N-oxide product. It is seen that at around 7 ps, the sulfur atom is oxidized (blue curve), and in a concerted event, the P-S bond elongates, increasing the likelihood of hydrolysis at the phosphorous atomic center (see red curve).

b. VX basic hydrolysis.

FPMD condensed phase metadynamics simulations of base hydrolysis were performed by randomly placing a single hydroxide anion (OH^-) to the core-ensemble of VX described in section III. Here the CV used is described in IIIb. Our calculations show that as the S-C bond is being "stretched," the S-C bond does not rupture until the OH^- anion diffuses close to the S-C bond. Figure 7 shows a strong correlation between the distance of the OH^- anion and the S-C bond (as determined by monitoring the distance between the S-C bond and OH^- anion), where the time evolution of the S-C bond distance (bottom curve) is correlated to the distance of the excess OH^- anion to the S-C bond (top curve). As can be seen, there is a strong correlation between when the S-C bond ruptures and the proximity of the excess OH^- anion; the S-C bond rupture takes places at ~6 ps into the simulation (as identified by the dotted vertical line). The S-C bond rupture free energy barrier was determined to be $\Delta G \approx 23$ kcal/mol, where experimentally this energy has been reported to be 25.7 kcal/mol,[15] in close agreement with our calculations.

c. VX autocatalitic hydrolysis.

In order to gain an understanding of the plausibility of "autocatalytic" hydrolysis[15,19,23] of VX (or R-VX), we performed FPMD metadynamic simulations of both a "gas-phase" (a small 'cluster' containing a single water and VX molecule; similar to that shown in Figure 8a) and fully condensed phase (using the core-ensemble described in section III) ensembles (see section IIIc for further details). Our gas-phase results identified the lowest PEB to be the hydrolysis reaction at the phosphorous atomic center, where the PEB was determined to be ~38 kcal/mol. Further, spontaneous protonation at the nitrogen atomic center was not seen, as implied from the illustration in Figure 8a.

Our condensed phase results however, show spontaneous protonation at the nitrogen atomic center and a concerted re-protonation of the newly formed hydroxide anion from an adjacent water molecule found in the first solvation shell (result confirmed from two independent calculations, which started from two very different starting configurations; see Figure 8b). Further, the newly produced hydroxide anion is found to tightly couple to the protonated nitrogen throughout the simulation (total simulation run time of >38 ps). Further hydrolysis at the phosphorus was not seen within the >38 ps simulation trajectory, where the corresponding reaction potential energy barrier, determined up to that point in the simulation, is greater than ~35 kcal/mol. Note that the resultant species remaining in the simulation ensemble after the protonation at the nitrogen atomic center are such that the simulations are effectively probing nucleophilic attack by water versus hydroxide ion, as proposed by Yang *et al.*[15,19] (see Figure 8c). These results are consistent with the slow reaction rates they report.

V. Conclusions

In this work, we have performed first-principles condensed phase simulations, which have elucidated a variety of important V-type nerve agent chemical reactions mechanisms and also illustrate the importance of treating the solvent explicitly. The decontamination mechanisms and chemical reaction energy barriers, as determined from our simulations, were found to be in good agreement with experiment for all mechanisms explored. Specifically, it was found that, 1) nitrogen centered decontamination reactions are energetically favorable and little difference is seen between VX and R-VX, 2) nitrogen oxidation promotes further oxidation at the sulfur atomic center and P-S bond rupture, 3) sulfur-center nucleophilic reactions were found to be facilitated by the presence of water in the "transition-state-structure," 4) carbon centered reactions were found to be energetically unfavorable, 5) P-centered nucleophilic substitution reactions lead to P-O or P-S bond cleavage, where

preference for P-O or P-S bond cleavage was found to depend on the orientation of the 'incoming' nucleophile, and 6) the autocatalytic hydrolysis mechanism of V-type nerve agents proposed by Yang *et al.* was not identified, but the experimentally determined slow reaction rates are consistent with the high PEB determined here.

The results shown here demonstrate the ability to accurately model chemical reaction mechanisms between chemical agents and decontamination solutions. Such an approach offers tremendous benefits in facilitating an understanding of decontamination chemistry in situations where traditional approaches are not feasible by suggesting the most favorable reaction pathways and likely reaction products. Though not suggested as a complete substitution for experimental work, the approach can be used to screen potential alternative decontamination solutions, if needed, and reduce the number of hazardous experiments to be performed by prioritizing the likely candidate solutions.

Acknowledgment. We thank the U. S. Department of Homeland Security Science and Technology Directorate for financial support. This work was performed under the auspices of the U.S. Department of Energy by Lawrence Livermore National Laboratory under Contract DE-AC52-07NA27344. We also would like to thank Livermore Computing for the copious amounts of computer time required to perform this work and Dennis Reutter for technical discussions of the results.

FIGURE CAPTIONS:

Figure 1: Chemical structure of VX (left) and R-VX (right).

Figure 2: The free energy profile as a function of the CV as determined from metadynamics simulation of the condensed phase reaction of VX and R-VX with ClO^-. The black (grey) lines represent a CV defined by the distance between the hypochlorite oxygen and the nitrogen (sulfur) atomic center of VX (dotted) and R-VX (solid); top panel. The lower panel is a snapshot of the simulation ensemble at the point labeled "(1)" in the upper panel, which is near the transition state for the VX/nitrogen reaction.

Figure 3: Illustration of the transition state structure of ClO- reaction at the sulfur atomic center for R-VX. As can be seen, the transition state is mediated by the presence of a single water molecule (the single water molecule is part of the transition state structure found for the S-centered reaction with ClO^-).

Figure 4: Illustration of the solvent mediated transition state structure of ClO- reaction to the sulfur atomic center for R-VX (right). The presence of a sterically hindered transition state structure is illustrated for VX (left).

Figure 5: Total energy along the IT-NEB optimized path for the reaction of OCl^- anion with the sulfur atomic center of VX (solid) and R-VX (dotted). Converged elastic bands with 32 movable replicas are shown.

Figure 6: Schematic representation of the VX/ hypochlorite reaction mechanism (panel a). Time evolution of VX reaction mechanism; atomic center distances along the simulation trajectory are plotted (panel b); hypoclorite oxidation reaction at the 'N' (black curve) and 'S'

(blue curve) atomics centers of VX. The 'P-S' bond distance during the reaction (red curve) is shown illustrating the occurrence of the P-S bond elongation after the sulfur is oxidized.

Figure 7: Correlation of OH^- anion to S-C bond rupture as a function of FPMD simulation time. Top panel represents of distance between the S-C bond and the hydroxide (OH^-) anion; the bottom panel represents the S-C bond distance. The dotted line represents the time in which the S-C bond begins to rupture. It is evident that the proximity of the OH^- anion is strongly correlated to the time in which the S-C bond ruptures.

Figure 8: Illustration of intramolecular amino group catalyzed hydrolysis of VX proposed in Ref. [15,19,23] (panel a). Illustration of what was seen in our simulations; (panel b) spontaneous protonation intermediate and (panel c) final reaction species in the simulation ensemble (see discussion section for details).

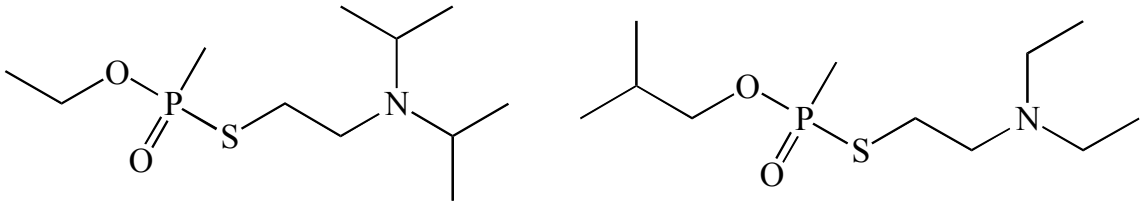

Figure 1

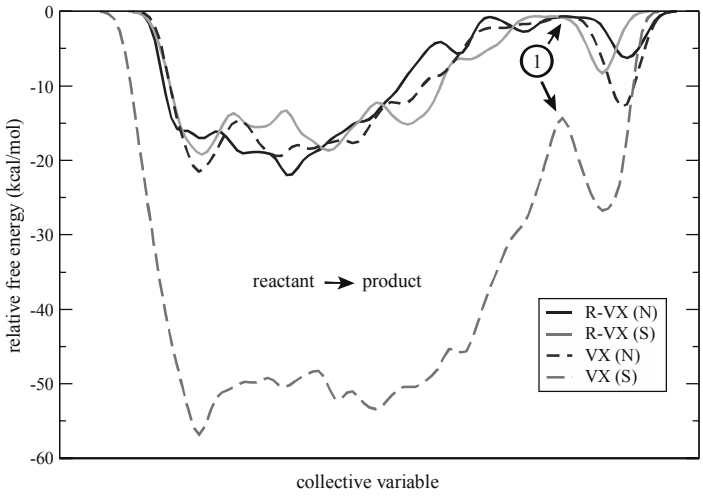
0
-10
-20
-30
-40
-50
-60
relative free energy (kcal/mol)
collective variable
reactant → product
1
R-VX (N)
R-VX (S)
VX (N)
VX (S)

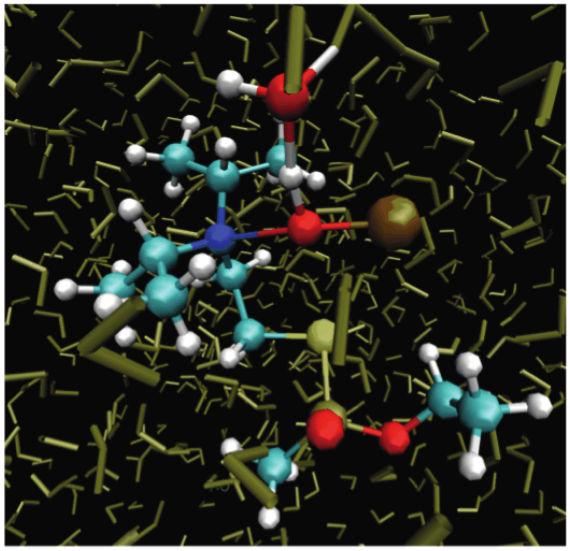

Figure 2

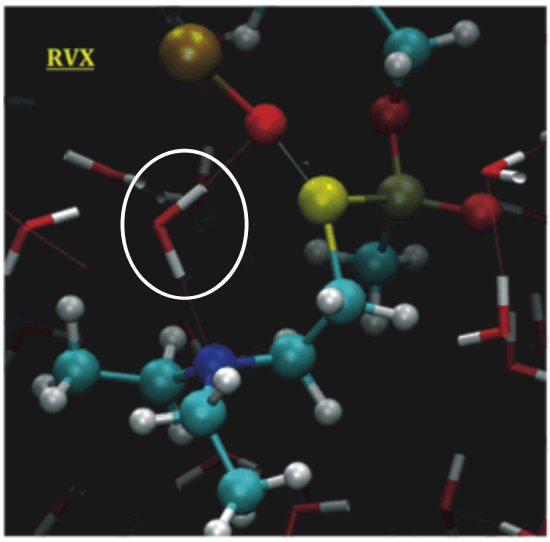

Figure 3

VX

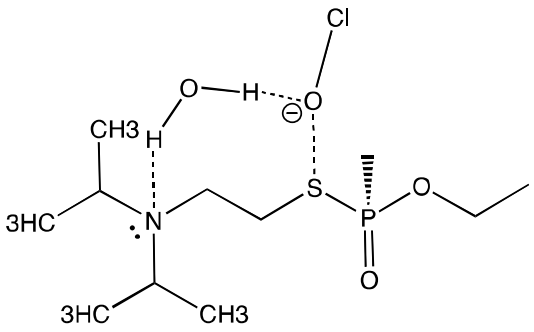

R-VX

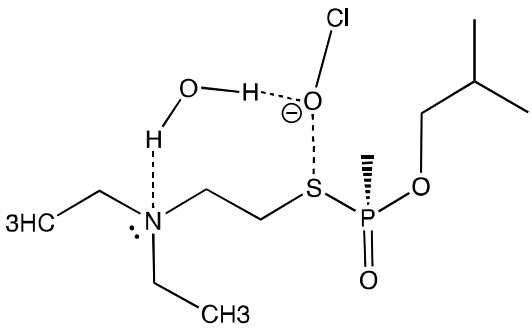

Figure 4

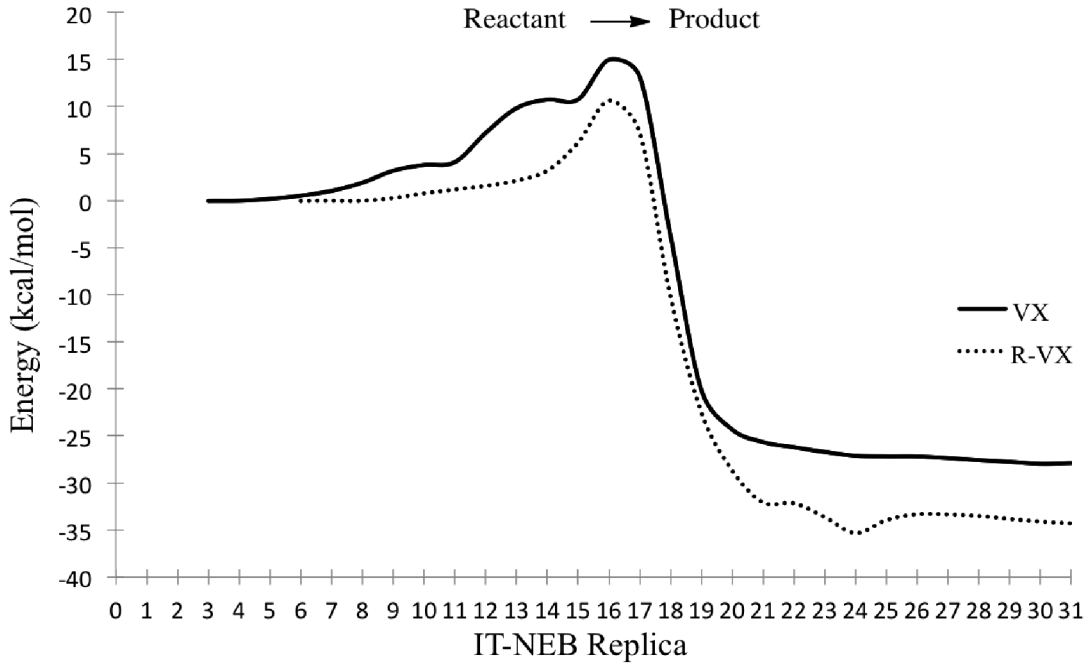
Reactant
Product
Energy (kcal/mol)
20
15
10
5
0
-5
-10
-15
-20
-25
-30
-35
-40
0 1 2 3 4 5 6 7 8 9 10 11 12 13 14 15 16 17 18 19 20 21 22 23 24 25 26 27 28 29 30 31
IT-NEB Replica
VX
R-VX

Figure 5

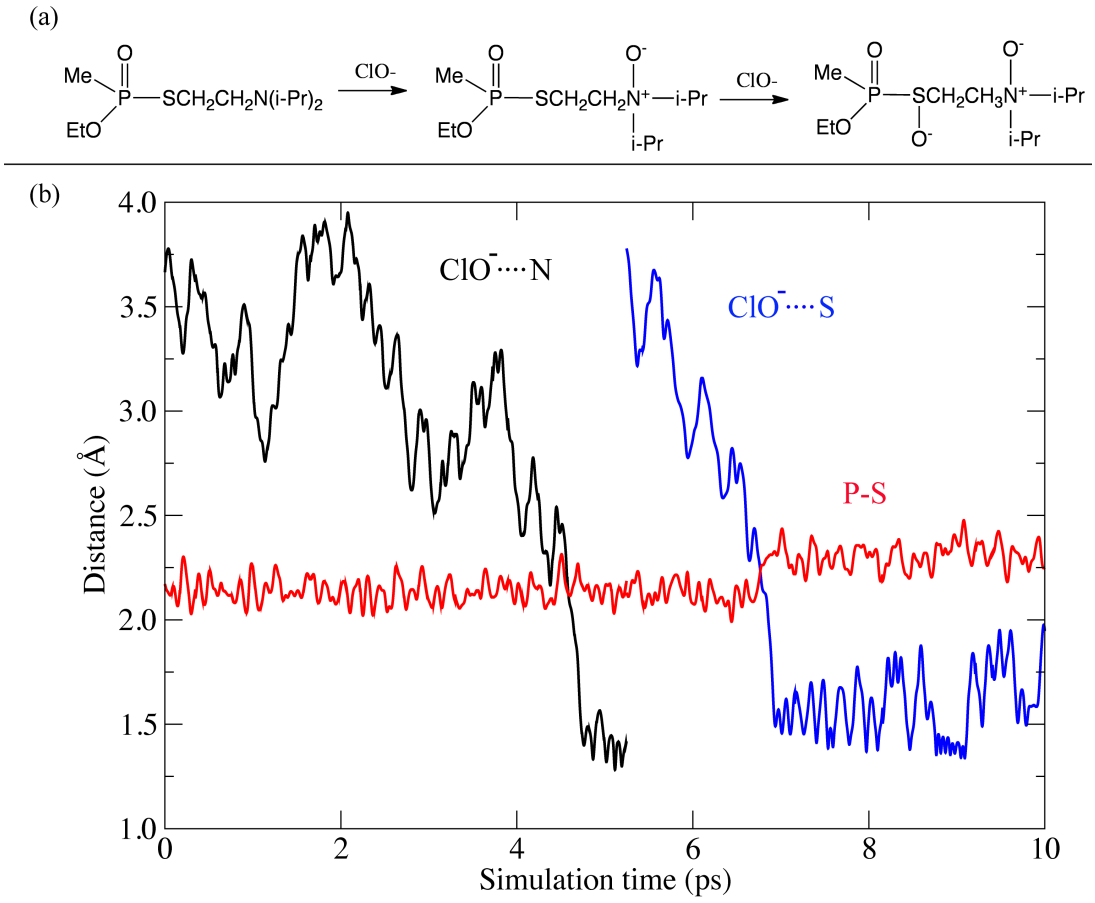
(a)
Me
O
P
EtO
SCH2CH2N(i-Pr)2
ClO-
SCH2CH2N+—i-Pr
i-Pr
O-
SCH2CH3N+—i-Pr
(b)
ClO-····N
ClO-····S
P-S
Distance (Å)
Simulation time (ps)
4.0
3.5
3.0
2.5
2.0
1.5
1.0
0
2
4
6
8
10

Figure 6

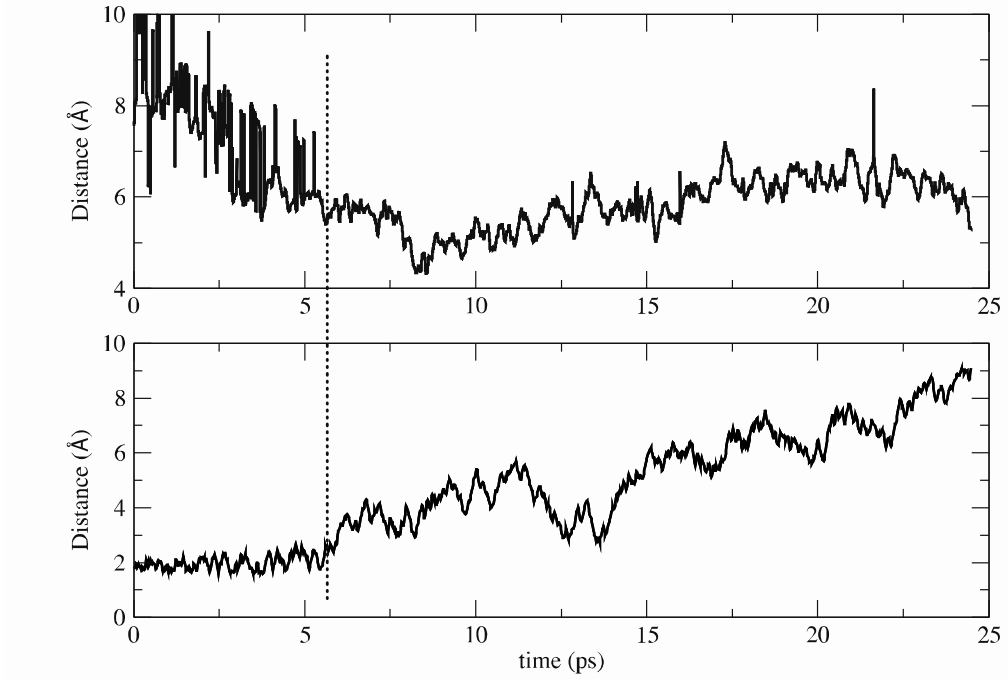
Distance (Å)
10
8
6
4
0
5
10
15
20
25
Distance (Å)
10
8
6
4
2
0
0
5
10
15
20
25
time (ps)

Figure 7

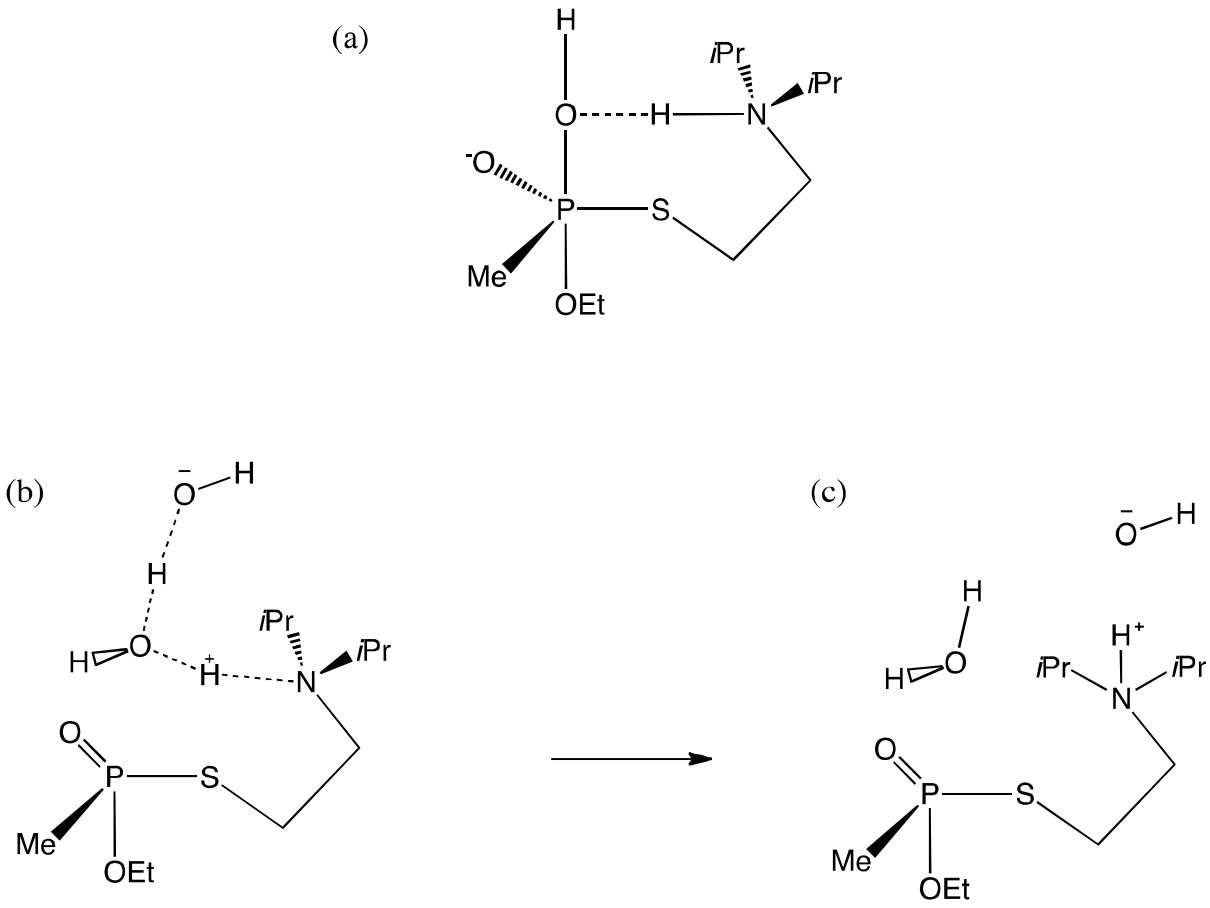
(a)
H
iPr
iPr
O
H
N
O
P
S
Me
OEt
(b)
O
H
H
O
H
iPr
iPr
H
N
O
P
S
Me
OEt
(c)
O
H
H
O
H
H
iPr
iPr
N
O
P
S
Me
OEt

Figure 8

TABLES:

Table 1: Calculated hypochlorite VX (VXH^+) and R-VX ($R\text{-}VXH^+$) reaction PEBs.[a]

	VX	**R-VX**	**VXH^+**	**$R\text{-}VXH^+$**
$P\text{-}OC_2H_5$	12 *(14.6/11.1)*	12 *(11.6)*	---	----
P-S	12 (15*) *(14.5/12.6)*	12 *(14.9)*	15*	12
S-C	23** *(25.7)*	---	---	---
N	12*	10*	32	37
S	15*	11*	48	14*

[a] Energies reported in kcal/mol. "Un-marked" numbers are determined from metadynamics sampling (see section IIIa). Experimental values for base hydrolysis are *italicized*, where the 'upper' number was determined at pH 12 and the 'lower' number at pH 11.[17,20] *As determined from IT-NEB sampling. **Results from our "base hydrolysis" metadynamics simulations (see section IIIb). The numbers "12(15)" in the VX(P-S) table entry represent reaction mechanisms where the –SR moiety is in either the equatorial or axial position in the trigonal bipyramidal transition state structure, respectively. All hypochlorite reactions centered at the carbon atoms in the V-type molecule backbone were found to have potential energy barriers of greater than 40 kcal/mol.

REFERENCES:

(1) Grote, R. F.; Hynes, J. T. *J Chem Phys* **1980**, *73*, 2715.
(2) Martinez, A. G.; Vilar, E. T.; Barcina, J. O.; Cerero, S. D. *J Org Chem* **2005**, *70*, 10238.
(3) Chen, X.; Brauman, J. I. *J Am Chem Soc* **2008**, *130*, 15038.
(4) Henkelman, G.; Jonsson, H. *J Chem Phys* **2000**, *113*, 9978.
(5) Laio, A.; Rodriguez-Fortea, A.; Gervasio, F. L.; Ceccarelli, M.; Parrinello, M. *J Phys Chem B* **2005**, *109*, 6714.
(6) Tu, A. T. *Natural and Selected Synthetic Toxins* **2000**, *745*, 304.
(7) Seckute, J.; Menke, J. L.; Emnett, R. J.; Patterson, E. V.; Cramer, C. J. *J Org Chem* **2005**, *70*, 8649.
(8) Daniel, K. A.; Kopff, L. A.; Patterson, E. V. *J Phys Org Chem* **2008**, *21*, 321.
(9) Khan, M. A. S.; Kesharwani, M. K.; Bandyopadhyay, T.; Ganguly, B. *J Mol Graph Model* **2009**, *28*, 177.
(10) Munro, N. B.; Talmage, S. S.; Griffin, G. D.; Waters, L. C.; Watson, A. P.; King, J. F.; Hauschild, V. *Environ Health Persp* **1999**, *107*, 933.
(11) McAnoy, A. M.; Williams, J.; Paine, M. R. L.; Rogers, M. L.; Blanksby, S. J. *J Org Chem* **2009**, *74*, 9319.
(12) Richardson, D. D.; Caruso, J. A. *Abstr Pap Am Chem S* **2006**, *231*.
(13) Richardson, D. D.; Caruso, J. A. *Anal Bioanal Chem* **2007**, *388*, 809.
(14) Cassagne, T.; Cristau, H. J.; Delmas, G.; Desgranges, M.; Lion, C.; Magnaud, G.; Torreilles, E.; Virieux, D. *Heteroatom Chem* **2001**, *12*, 485.
(15) Yang, Y. C. *Accounts Chem Res* **1999**, *32*, 109.
(16) Yang, Y. C.; Baker, J. A.; Ward, J. R. *Chemical Reviews* **1992**, *92*, 1729.
(17) Yang, Y. C.; Szafraniec, L. J.; Beaudry, W. T.; Rohrbaugh, D. K.; Samuel, J. B. In *Proceedings of the Novermber 1994 ERDEC Scientific Conference of Chemical and Biological Defense Research;* Aberdeen Proving Ground, MD, 1996, p 375.
(18) Yang, Y. C.; Szafraniec, L. L.; Beaudry, W. T.; Rohrbaugh, D. K. *J Am Chem Soc* **1990**, *112*, 6621.
(19) Yang, Y. C.; Szafraniec, L. L.; Beaudry, W. T.; Rohrbaugh, D. K.; Procell, L. R.; Samuel, J. B. *J Org Chem* **1996**, *61*, 8407.
(20) Szafraniec, L. L.; Beaudry, W. T.; Szafraniec, L. J. In *Proceedings of the ERDEC Scientific Conference on Chemical and Biological Defence Research* 1995, p 885.
(21) Groenewold, G. S.; Williams, J. M.; Appelhans, A. D.; Gresham, G. L.; Olsbn, J. E.; Jeffery, M. T.; Rowland, B. *Environ Sci Technol* **2002**, *36*, 4790.
(22) Williams, J. M.; Rowland, B.; Jeffery, M. T.; Groenewold, G. S.; Appelhans, A. D.; Gresham, G. L.; Olson, J. E. *Langmuir* **2005**, *21*, 2386.
(23) Yang, Y. C. *Chem Ind-London* **1995**, 334.
(24) http://cp2k.berlios.de.
(25) VandeVondele, J.; Krack, M.; Mohamed, F.; Parrinello, M.; Chassaing, T.; Hutter, J. *Comput Phys Commun* **2005**, *167*, 103.
(26) Goedecker, S.; Teter, M.; Hutter, J. *Phys Rev B* **1996**, *54*, 1703.
(27) Perdew, J. P.; Burke, K.; Ernzerhof, M. *Phys Rev Lett* **1996**, *77*, 3865.
(28) Martyna, G. J.; Klein, M. L.; Tuckerman, M. *J Chem Phys* **1992**, *97*, 2635.
(29) Laio, A.; Parrinello, M. *P Natl Acad Sci USA* **2002**, *99*, 12562.
(30) Micheletti, C.; Laio, A.; Parrinello, M. *Phys Rev Lett* **2004**, *92*.
(31) Gervasio, F. L.; Parrinello, M.; Ceccarelli, M.; Klein, M. L. *J Mol Biol* **2006**, *361*, 390.

(32) Lee, J. G.; Asciutto, E.; Babin, V.; Sagui, C.; Darden, T.; Roland, C. *J Phys Chem B* **2006**, *110*, 2325.
(33) Gervasio, F. L.; Laio, A.; Parrinello, M. *J Am Chem Soc* **2005**, *127*, 2600.
(34) Epstein, J.; Callahan, J. J.; Bauer, V. E. *Phosphorus* **1974**, *4*, 157.
(35) http://accelrys.com/.
(36) Sun, H. *J Phys Chem B* **1998**, *102*, 7338.
(37) Such an effect would likely be manifest in the pre- exponential factor, A, in the 'Arrhenius equation,' which may be thought of as the attempt frequency of the reaction.
(38) Michalowicz, J.; Duda, W.; Stufka-Olczyk, J. *Chemosphere* **2007**, *66*, 657.
(39) Zheng, F.; Zhen, C. G.; Ornstein, R. L. *J Chem Soc Perk T 2* **2001**, 2355.
(40) Van Bochove, M. A.; Swart, M.; Bickelhaupt, F. M. *J Am Chem Soc* **2006**, *128*, 10738.
(41) van Bochove, M. A.; Bickelhaupt, F. M. *Eur J Org Chem* **2008**, 649.
(42) van Bochove, M. A.; Swart, M.; Bickelhaupt, F. M. *Chemphyschem* **2007**, *8*, 2452.
(43) Cavell, R. G.; Gibson, J. A.; The, K. I. *Inorg Chem* **1978**, *17*, 2880.
(44) Jackson, C. J.; Liu, J. W.; Coote, M. L.; Ollis, D. L. *Org Biomol Chem* **2005**, *3*, 4343.